Universal amplitude ratios from numerical studies of the three-dimensional $O(2)$ model



2002 J. Phys. A: Math. Gen. 35 6517

(http://iopscience.iop.org/0305-4470/35/31/301)

INSTITUTE OF PHYSICS PUBLISHING JOURNAL OF PHYSICS A: MATHEMATICAL AND GENERAL

J. Phys. A: Math. Gen. **35** (2002) 6517–6543 PII: S0305-4470(02)33875-7

# Universal amplitude ratios from numerical studies of the three-dimensional $O(2)$ model

**A Cucchieri[1], J Engels[2], S Holtmann[2], T Mendes[1] and T Schulze[2]**

[1] IFSC-USP, Caixa postal 369, 13560-970 São Carlos SP, Brazil
[2] Fakultät für Physik, Universität Bielefeld, D-33615 Bielefeld, Germany

E-mail: engels@physik.uni-bielefeld.de, holtmann@physik.uni-bielefeld.de, tschulze@physik.uni-bielefeld.de, cucchieri@if.sc.usp.br and mendes@if.sc.usp.br

Received 15 February 2002, in final form 7 June 2002
Published 26 July 2002
Online at stacks.iop.org/JPhysA/35/6517

**Abstract**

We investigate the three-dimensional $O(2)$ model near the critical point by Monte Carlo simulations and calculate the major universal amplitude ratios of the model. The ratio $U_0 = A^+/A^-$ is determined directly from the specific heat data at zero magnetic field. The data do not, however, allow us to extract an accurate estimate for $\alpha$. Instead, we establish a strong correlation of $U_0$ with the value of $\alpha$ used in the fit. This numerical $\alpha$-dependence is given by $A^+/A^- = 1 - 4.20(5)\alpha + O(\alpha^2)$. For the special $\alpha$-values used in other calculations, we find full agreement with the corresponding ratio values, e.g. that of the shuttle experiment with liquid helium. On the critical isochore, we obtain the ratio $\xi^+/\xi_T^- = 0.293(9)$, and on the critical line the ratio $\xi_T^c/\xi_L^c = 1.957(10)$ for the amplitudes of the transverse and longitudinal correlation lengths. These two ratios are independent of the $\alpha$- or $\nu$-values used here.

PACS numbers: 64.60.Cn, 75.40., 05.50+q, 05.10.Ln, 02.60.Cb

## 1. Introduction

In quantum field theory and condensed matter physics $O(N)$ symmetric vector models play an essential part, because they are representatives of universality classes for many physical systems. The universal properties of the $O(N)$ models—the critical exponents and amplitude ratios, which describe the critical phenomena—are therefore of considerable importance. In three dimensions, the case $N = 2$ is a special one: it is the first vector model (with increasing $N$) showing Goldstone effects, and the exponent $\alpha$, which controls the critical behaviour of the specific heat, is very close to zero. In fact, if one plots $\alpha$ versus $N$, as determined by field theory methods [1–4], then the function is approximately linear in $N$ and becomes negative just below $N = 2$. The proximity of $\alpha$ to zero also made it difficult to determine the type of

  

singularity for the specific heat in real systems. Indeed, for the lambda transition of helium a nearly logarithmic singularity (corresponding to $\alpha = 0$) was first measured [5] and a similar behaviour was found at the gas–liquid critical point [6]. However, with the experimental precision reached nowadays, especially that of the spectacular shuttle experiment with liquid helium [7, 8], there is no doubt that the critical exponent $\alpha$ is very small, but non-zero, and because it is negative the peak of the specific heat is finite.

In this paper we calculate, among other quantities, the specific heat from Monte Carlo simulations. The determination of $\alpha$ from these data poses, as we shall see, similar problems as in experiments. Of course, there is only one value of $\alpha$ for the 3D $O(2)$-universality class, but it is unclear what the correct value is (see e.g. the survey in table 19 of [9]). We therefore pursue the strategy of calculating the universal ratios from our data for different $\alpha$-values in the range where the actual value most probably is. The strongest dependence on the $\alpha$ used is expected for fits involving the universal amplitude ratio $A^+/A^-$ of the specific heat. The same is true for all theoretical determinations [10, 11] of this ratio. Apart from $A^+/A^-$ we derive from our simulations other universal quantities and amplitude ratios, which characterize the $O(2)$-universality class in three dimensions.

The model which we investigate is the standard $O(2)$-invariant nonlinear $\sigma$-model (or $XY$ model), which is defined by

$$\beta\mathcal{H} = -J \sum_{\langle x,y \rangle} \vec{\phi}_x \cdot \vec{\phi}_y - \vec{H} \cdot \sum_x \vec{\phi}_x. \tag{1}$$

Here $x$ and $y$ are the nearest-neighbour sites on a three-dimensional hypercubic lattice, $\vec{\phi}_x$ is a two-component unit vector at site $x$ and $\vec{H}$ is the external magnetic field. We consider the coupling constant $J$ as inverse temperature, that is $J = 1/T$. Instead of fixing the length of the spin vectors $\vec{\phi}_x$ to 1 we could have introduced an additional term $\sum_x \left[\vec{\phi}_x^2 + \lambda\left(\vec{\phi}_x^2 - 1\right)^2\right]$ on the right-hand side of equation (1). By choosing an appropriate $\lambda$ value [12] it is then possible to eliminate leading-order corrections to scaling. As it will turn out, these corrections are negligible in the energy density and marginal in the specific heat also with the Hamiltonian from equation (1). Moreover, we want to combine amplitudes obtained from former simulations at non-zero magnetic field [13] using the same Hamiltonian with the amplitudes we determine now in order to calculate universal ratios.

As long as $H = |\vec{H}|$ is non-zero, one can decompose the spin vector $\vec{\phi}_x$ into a longitudinal (parallel to the magnetic field $\vec{H}$) and a transverse component,

$$\vec{\phi}_x = \phi_x^{\parallel} \vec{e}_H + \vec{\phi}_x^{\perp}, \qquad \text{with} \quad \vec{e}_H = \vec{H}/H. \tag{2}$$

The order parameter of the system, the magnetization $M$, is then the expectation value of the lattice average $\phi^{\parallel}$ of the longitudinal spin component,

$$M = \left\langle \frac{1}{V} \sum_x \phi_x^{\parallel} \right\rangle = \langle \phi^{\parallel} \rangle. \tag{3}$$

Here, $V = L^3$ and $L$ is the number of lattice points per direction. There are two types of susceptibilities. The longitudinal susceptibility is defined as usual by the derivative of the magnetization, whereas the transverse susceptibility corresponds to the fluctuation of the lattice average $\vec{\phi}^{\perp}$ of the transverse spin component,

$$\chi_L = \frac{\partial M}{\partial H} = V(\langle \phi^{\parallel 2} \rangle - M^2) \tag{4}$$

$$\chi_T = V \langle \vec{\phi}^{\perp 2} \rangle. \tag{5}$$

The total magnetic susceptibility is

$$\chi = \chi_L + \chi_T. \tag{6}$$

At zero magnetic field, $H = 0$, there is no longer a preferred direction and the lattice average of the spins

$$\vec{\phi} = \frac{1}{V}\sum_x \vec{\phi}_x \tag{7}$$

will have a vanishing expectation value on all finite lattices, $\langle\vec{\phi}\rangle = 0$; the longitudinal and transverse susceptibilities become equal for $T > T_c$ and diverge for $T < T_c$ because of the Goldstone modes [13]. Nevertheless we can use $\vec{\phi}$ to define the total susceptibility and the Binder cumulant by

$$\chi = V\langle\vec{\phi}^2\rangle \tag{8}$$

$$g_r = \frac{\langle(\vec{\phi}^2)^2\rangle}{\langle\vec{\phi}^2\rangle^2} - 3. \tag{9}$$

For $T > T_c$ we have $\chi = 2\chi_L = 2\chi_T$. We approximate the order parameter $M$ for $H = 0$ by [14]

$$M \simeq \langle|\vec{\phi}|\rangle. \tag{10}$$

On finite lattices, the magnetization of equation (10) approaches the infinite volume limit from above, whereas $M$ as defined by equation (3) for $H \neq 0$ reaches the thermodynamic limit from below.

In our zero field simulations, we want to measure three further observables: the energy density, the specific heat and the correlation length. The energy of a spin configuration is simply

$$E = -\sum_{\langle x,y\rangle} \vec{\phi}_x \cdot \vec{\phi}_y \tag{11}$$

and the energy density $\epsilon$ is then

$$\epsilon = \langle E\rangle/V. \tag{12}$$

For the specific heat $C$ we obtain

$$C = \frac{\partial\epsilon}{\partial T} = \frac{J^2}{V}(\langle E^2\rangle - \langle E\rangle^2). \tag{13}$$

The second moment correlation length is calculated from the formula

$$\xi_{2\mathrm{nd}} = \left(\frac{\chi/F - 1}{4\sin^2(\pi/L)}\right)^{1/2} \tag{14}$$

where $F$ is the Fourier transform of the correlation function at momentum $p_\mu = 2\pi\hat{e}_\mu/L$, and $\hat{e}_\mu$ a unit vector in one of the three directions,

$$F = \frac{1}{V}\left\langle\left|\sum_x \exp(\mathrm{i}p_\mu x)\vec{\phi}_x\right|^2\right\rangle. \tag{15}$$

In the simulations, we compute $F$ from an average over all three directions. Strictly speaking, equation (14) can only serve as a definition of the correlation length for $T > T_c$, because the

exponential correlation length diverges for $H \to 0$ and $T < T_c$. Instead, it is possible to introduce a transverse correlation length $\xi_T$ on the coexistence line [15], which is connected to the so-called stiffness constant $\rho_s$ for $d = 3$ by

$$\xi_T = \rho_s^{-1} \qquad \text{for} \quad H = 0 \quad T < T_c. \tag{16}$$

We explain later how to calculate $\rho_s$. For $H \neq 0$ there are two exponential correlation lengths, a transverse ($\xi_T$) and a longitudinal one ($\xi_L$). Their second moment forms may be computed again from equation (14) by replacing $\chi$ and $F$ with their respective transverse or longitudinal counterparts.

The rest of the paper is organized as follows. First, we discuss the critical behaviour of the observables and define the universal amplitude ratios, which we want to determine. In section 3 we describe our simulations at $H = 0$, the results for the Binder cumulant, the critical point and the correlation length. Then we analyse the data for the energy and the specific heat. In section 4 we discuss as an alternative the calculation of $A^+/A^-$ from the equation of state, which was obtained from non-zero field simulations. Section 5 serves to find the specific heat and the correlation lengths at $T_c$, as well as the stiffness constant, from $H \neq 0$ simulations. We close with a summary of the ratios and the conclusions.

## 2. Critical behaviour

In the thermodynamic limit ($V \to \infty$) the observables show power law behaviour close to $T_c$. It is described by critical amplitudes and exponents of the reduced temperature $t = (T - T_c)/T_c$. Note that we use here another definition of $t$ than in [13]. We will mention this point again later. The scaling laws at $H = 0$ are
for the magnetization

$$M = B(-t)^{\beta} \qquad \text{for} \quad t < 0 \tag{17}$$

for the longitudinal susceptibility

$$\chi_L = C^+ t^{-\gamma} \qquad \text{for} \quad t > 0 \tag{18}$$

for the transverse correlation length

$$\xi_T = \xi_T^- (-t)^{-\nu} \qquad \text{for} \quad t < 0 \tag{19}$$

for the correlation length

$$\xi = \xi^+ t^{-\nu} \qquad \text{for} \quad t > 0 \tag{20}$$

for $t \to \pm 0$ the energy density

$$\epsilon = \epsilon_{ns} + T_c t \left( C_{ns} + \frac{A^{\pm}}{\alpha(1-\alpha)} |t|^{-\alpha} \right) \tag{21}$$

and the specific heat

$$C = C_{ns} + \frac{A^{\pm}}{\alpha} |t|^{-\alpha}. \tag{22}$$

The specific heat and the energy density contain non-singular terms $C_{ns}$ and $\epsilon_{ns}$, which are due to derivatives of the analytic part $f_{ns}$ of the free energy density. They are the values of the specific heat and energy density at $T_c$. With our definition for the specific heat amplitudes, we have already singled out their main $\alpha$-dependences, the remaining factors $A^{\pm}$ are only moderately varying with $\alpha$.

On the critical line $T = T_c$ or $t = 0$ we have for $H > 0$ the scaling laws

$$M = d_c H^{1/\delta} \qquad \text{or} \qquad H = D_c M^{\delta} \tag{23}$$

and for the longitudinal and transverse correlation lengths $\xi_{L,T}$

$$\xi_{L,T} = \xi^c_{L,T} H^{-\nu_c} \qquad \nu_c = \nu/\beta\delta. \tag{24}$$

The specific heat scales as

$$C = C_{ns} + \frac{A_c}{\alpha_c} H^{-\alpha_c} \qquad \alpha_c = \alpha/\beta\delta. \tag{25}$$

We assume the following hyperscaling relations among the critical exponents to be valid:

$$2 - \alpha = \mathrm{d}\nu \qquad \gamma = \beta(\delta - 1) \qquad \mathrm{d}\nu = \beta(1 + \delta). \tag{26}$$

As a consequence, only two critical exponents are independent. Because of the hyperscaling relations and the already implicitly assumed equality of the critical exponents above and below $T_c$, one can construct a multitude of universal amplitude ratios [15] (see also the discussion in [9]). The following list of ratios contains those which we want to determine here,

$$U_0 = A^+/A^- \qquad U_\xi = \xi^+/\xi^-_T \tag{27}$$

$$R^+_\xi = (A^+)^{1/d}\xi^+ \qquad R^T_\xi = (A^-)^{1/d}\xi^-_T \tag{28}$$

$$R_\chi = C^+ D_c B^{\delta-1} \qquad R_C = A^+ C^+/B^2 \tag{29}$$

and

$$R_A = A_c D_c^{-(1+\alpha_c)} B^{-2/\beta} \qquad Q^T_2 = \left(\xi^c_T/\xi^+\right)^{\gamma/\nu} C^+/d_c(1/\delta + 1). \tag{30}$$

One of the ratios, $R_\chi$, was already calculated by us from non-zero magnetic field simulations [13], using the exponents of [12]. We found

$$R_\chi = 1.356(4). \tag{31}$$

In order to normalize the equation of state, the temperature and the magnetic field in the same paper, we computed the critical amplitudes of the magnetization on the coexistence line and the critical line with the result

$$B = \hat{B} T_c^{\beta} = 1.245(7) \qquad d_c = 0.978(2) \quad D_c = 1.11(1) \tag{32}$$

where $\hat{B} = 0.945(5)$. The value for $J_c = T_c^{-1} = 0.454\,165$ was taken from [16].

## 3. Simulations at $H = 0$

All our simulations were done on three-dimensional lattices with periodic boundary conditions. As in [13] we have used the Wolff single cluster algorithm. The main part of the $H = 0$ data was taken from lattices with linear extensions $L = 24, 36, 48, 72, 96$ and 120. Between the measurements, we performed 300–800 cluster updates to reduce the integrated autocorrelation time $\tau_{\mathrm{int}}$. Apart from the largest lattice ($L = 120$) where we made runs only at six couplings, we generally scanned the neighbourhood of $J_c$ by runs at more than 30 points on each lattice, with special emphasis on the region $0.454\,14 \leqslant J \leqslant 0.454\,19$. This enabled a

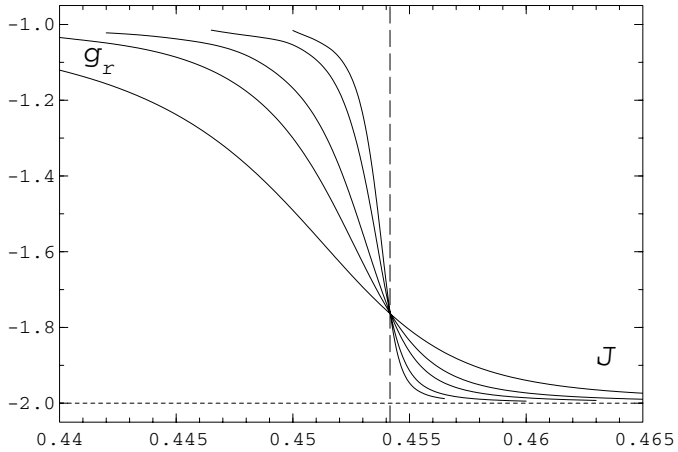


**Figure 1.** The Binder cumulant $g_r$ from equation (9) as a function of the coupling $J$. The curves were obtained by reweighting the data. With increasing lattice size $L = 24$, 36, 48, 72 and 96, the slope of the respective curve increases close to the critical point. The vertical dashed line denotes $J_c$ from [16].

**Table 1.** Survey of the Monte Carlo simulations at $H = 0$ for different lattices. Here $N_J$ is the number of different couplings at which runs were performed; $\tau_{\text{int}}$ is the integrated autocorrelation time for the energy and $N_{\text{meas}}$ the number of measurements per coupling in units of 1000.

| $L$ | $J$-range | $N_J$ | $N_{\text{meas}}$ (1000) | $\tau_{\text{int}}$ ($t < 0$) | $\tau_{\text{int}}$ ($t \approx 0$) | $\tau_{\text{int}}$ ($t > 0$) |
|---|---|---|---|---|---|---|
| 24 | 0.440–0.4675 | 35 | $\geqslant$100 | 1–3 | 1–3 | 1–3 |
| 36 | 0.440–0.4650 | 43 | $\geqslant$100 | 1–4 | 2–3 | 2–10 |
| 48 | 0.442–0.4650 | 55 | $\geqslant$100 | 1–5 | 2–5 | 4–13 |
| 72 | 0.4465–0.460 | 41 | 80–100 | 1–4 | 4–8 | 7–21 |
| 96 | 0.450–0.4567 | 33 | 60–80 | 2–10 | 6–7 | 7–35 |
| 120 | 0.452–0.4562 | 6 | 20 | 2–4 | 14 | 12–23 |

comfortable reweighting analysis of the data. More details of these simulations are presented in table 1.

### *3.1. The critical point and the Binder cumulant*

It is obvious that any determination of critical amplitudes relies crucially on the exact location of the critical point. Since we have produced a considerable number of data in the neighbourhood of the critical point, it was natural to verify first the rather precise result of Ballesteros *et al* [16]. We have done this by studying the Binder cumulant $g_r$, which is directly a finite-size-scaling function:

$$g_r = Q_g(tL^{1/\nu}, L^{-\omega}). \tag{33}$$

The function $Q_g$ depends on the thermal scaling field and on possible irrelevant scaling fields. Here we have specified only the leading irrelevant scaling field proportional to $L^{-\omega}$, with $\omega > 0$. At the critical point, $t = 0$, $g_r$ should therefore be independent of $L$ apart from corrections due to these irrelevant scaling fields. In figure 1 we show our results for $g_r$ as obtained by reweighting the direct data. We observe, at least on the scale of figure 1, no deviation from the scaling hypothesis. However, after a blow-up of the close vicinity of the

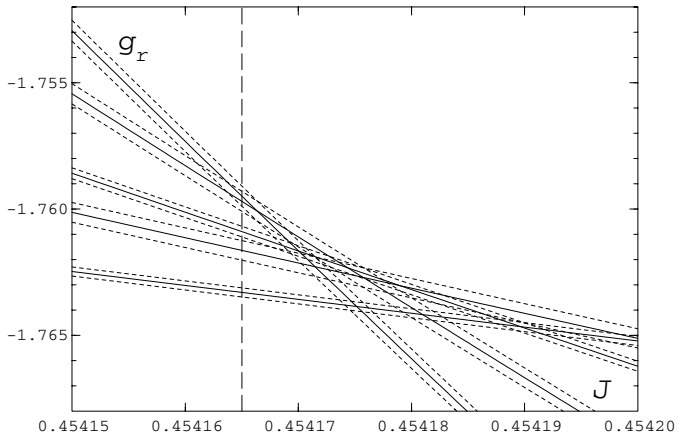


**Figure 2.** The Binder cumulant $g_r$ in the close neighbourhood of the critical point. The figure is an enlargement of figure 1. The dashed lines accompanying the solid lines show the jackknife error corridor.

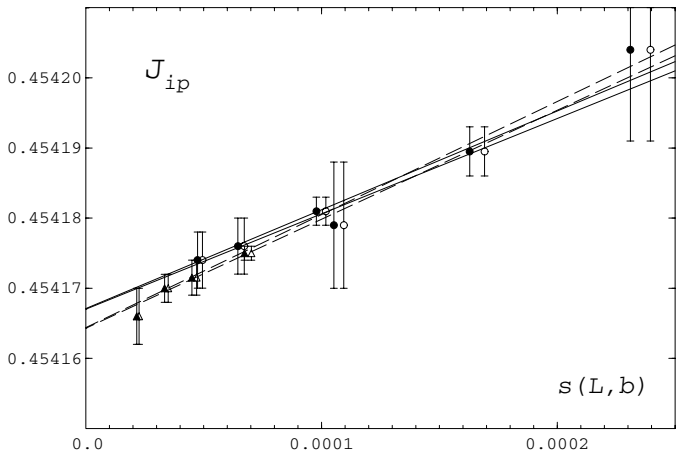


**Figure 3.** The coupling $J_{ip}$ at the intersection point of $g_r(L)$ and $g_r(bL)$ for various combinations of $L$ and $b$ as a function of $s(L,b)$, equation (34). The full (open) symbols were calculated with $\nu = 0.669$ (0.673). The dashed (solid) lines are linear fits with (without) the $L = 96$ intersection points, denoted here by triangles.

critical point, as shown in figure 2, we can see that the intersection points between curves from different lattices are not coinciding. The shift $\Delta J$ of the crossing point from the infinite volume critical coupling $J_c$ can be estimated by expanding the scaling function $Q_g$ to the lowest order in both variables. For two lattices with sizes $L$ and $L' = bL$ one gets

$$\Delta J^{L,L'} \propto s(L,b) = \frac{1-b^{-\omega}}{b^{1/\nu}-1} L^{-\omega-1/\nu}. \tag{34}$$

In figure 3 we have plotted the $J$-values of the intersection points for each pair of lattices as a function of the variable $s(L,b)$ of equation (34). For $\omega$ we used the value 0.79(2) of [12], and for $\nu$ we chose the two values $\nu = 0.669$ and 0.673 as bounds of the probable $\nu$-range. Of course, the intersection points are completely independent of $\nu$ and $\omega$. Only the

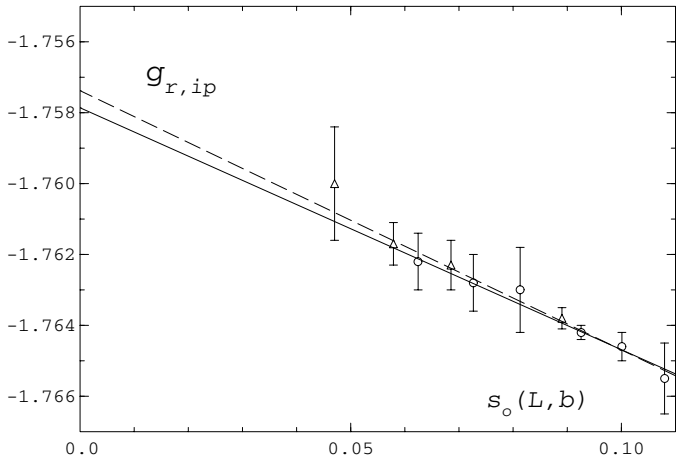


**Figure 4.** The Binder cumulant $g_{r,ip}$ at the intersection point for various combinations of $L$ and $b$ as a function of $s_o(L, b)$, equation (36). The dashed (solid) lines are linear fits with (without) the $L = 96$ intersection points, denoted here by triangles.

variable $s(L, b)$ changes when the exponents are changed. As can be seen in figure 3 also, the extrapolation to the critical point $J_c$ for $L \to 0$ (or $s(L, b) \to 0$) is unaffected by the choice of $\nu$. The same applies to a variation of $\omega$. Since the slope of $g_r(L = 96)$ close to the critical point is rather large, a small numerical uncertainty might shift the intersection points with the other curves considerably. We have therefore determined $J_c$ also by fits excluding the results from the largest lattice. Thus we arrive at the final estimate

$$J_c = 0.454\,167(4) \tag{35}$$

in full agreement with the result $J_c = 0.454\,165(4)$ of Ballesteros *et al* [16]. In order to be consistent with our previous papers, we use in the following again the value from [16].

In a similar manner, one can determine from the same data the universal value $g_r(J_c)$. Here the difference of the $g_r$-values at the intersection points to $g_r(J_c)$ is

$$\Delta g_r^{L,L'} \propto s_o(L, b) = \frac{b^{1/\nu} - b^{-\omega}}{b^{1/\nu} - 1} L^{-\omega}. \tag{36}$$

In figure 4 we show the extrapolation of $g_r$ to the critical point value at $s_o(L, b) = 0$. A variation of $\omega$ in the range 0.77–0.81 leads only to a shift of $10^{-4}$. The new variable $s_o(L, b)$ is practically independent of $\nu$; the influence of $\nu$ is not visible in figure 4. Comparing again extrapolations with and without the $L = 96$ points, one obtains

$$g_r(J_c) = -1.758(2) \qquad \text{or} \qquad \frac{\langle(\vec{\phi}^2)^2\rangle}{\langle\vec{\phi}^2\rangle^2}(J_c) = 1.242(2) \tag{37}$$

well in accord with the result of [11] (see also the long discussion in [17]).

### *3.2. The correlation length*

In our $H = 0$ simulations, we have measured the correlation length using the second moment formula, equation (14). The finite-size-scaling equation for $\xi$ is

$$\xi = L Q_\xi(t L^{1/\nu}, L^{-\omega}) \tag{38}$$

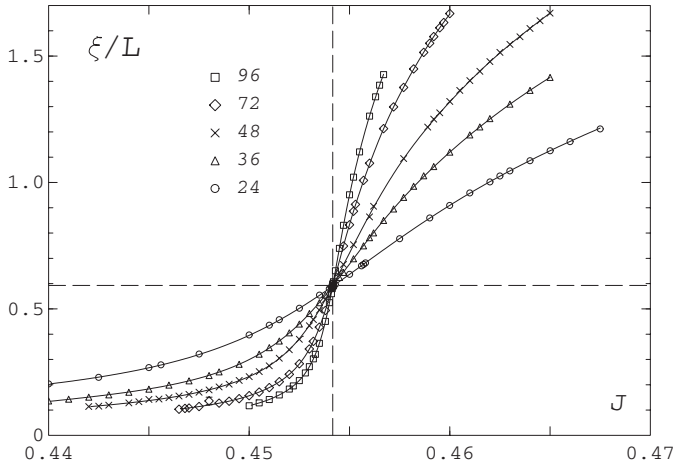


**Figure 5.** The correlation length $\xi$ divided by $L$ versus $J$ for $L = 24$, 36, 48, 72 and 96. The solid lines were calculated by reweighting the data. The dashed vertical line gives the position of $J_c$, and the horizontal one gives the universal value, equation (39).

and $\xi/L = Q_\xi$ is a scaling function such as $g_r$, that is its value at the critical point is universal for $L \to \infty$. In figure 5 we have plotted our correlation length data divided by $L$. Here formula (14) has also been evaluated for $J > J_c$ or $T < T_c$ though in this region the data cannot be identified with the correlation length. We see again that all curves intersect at the previously determined critical point. A closer look into the neighbourhood of $J_c$ reveals however similar corrections to scaling as in the case of $g_r$. The corresponding extrapolation of the variable $s_o(L, b)$ to zero leads for $\xi/L$ to

$$\xi/L\ (J_c) = 0.593(2). \tag{39}$$

This result confirms nicely the value $\xi/L = 0.5927$ from the preliminary simulations mentioned in [12].

Our data for the correlation length can also be used to find the critical amplitude $\xi^+$ of equation (20). To this end, we use a method described in detail in [18]. We briefly repeat the main arguments assuming for simplicity that there are no corrections to scaling. An observable $O$ with critical behaviour approaches for either positive or negative $t$ and $L \to \infty$ the limiting form

$$O_\infty = a_0|t|^{-\rho} \qquad \text{for} \quad |t| \to 0 \tag{40}$$

where $a_0$ is the critical amplitude and $\rho$ the critical exponent. At finite $L$ the observable satisfies a scaling relation

$$O(t, L) = L^{\rho/\nu} Q_O(x_t) \qquad \text{with} \quad x_t = tL^{1/\nu}. \tag{41}$$

Here, $Q_O$ is the finite-size-scaling function of $O$. In order to ensure the correct thermodynamic limit for fixed small $|t|$, we must have the relation

$$O_\infty = |t|^{-\rho} \lim_{x_t \to \pm\infty} |x_t|^\rho Q_O(x_t). \tag{42}$$

The sign of $x_t$ is of course the same as that of $t$. It is clear then, that the function

$$A_O(x_t) = |x_t|^\rho Q_O(x_t) \tag{43}$$

will converge asymptotically to the critical amplitude $a_0$. Moreover, $a_0$ will be an extreme value of $A_O(x_t)$.

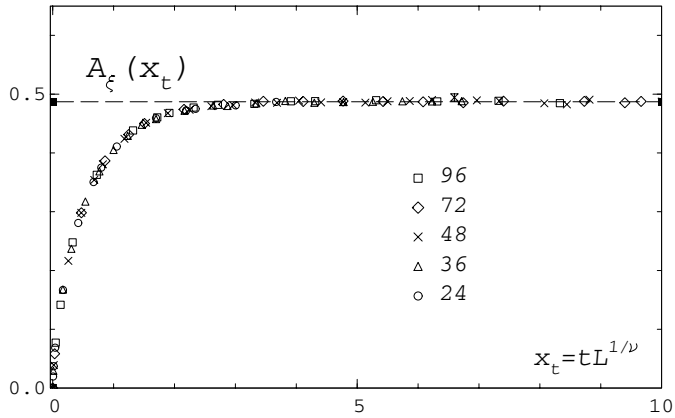


**Figure 6.** The amplitude function $A_\xi$, equation (43), of the correlation length versus the scaling variable $x_t$ for $\nu = 0.671$ and $L = 24, 36, 48, 72$ and 96. The horizontal line indicates the $\xi^+$-value.

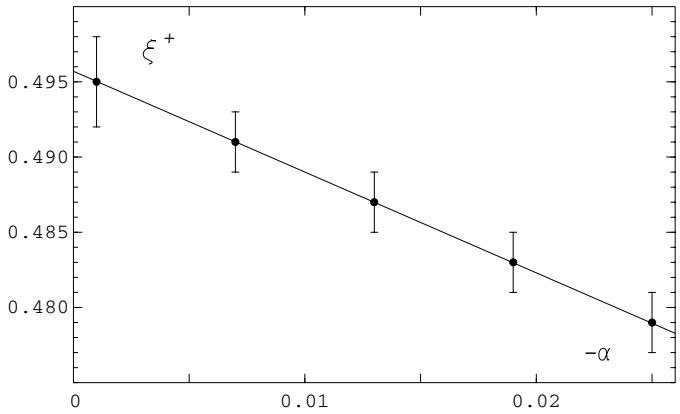


**Figure 7.** The critical amplitude $\xi^+$, equation (20), of the correlation length versus $-\alpha$. The data (circles) are determined from the amplitude function $A_\xi(x_t)$; the solid line is the linear fit (44).

We have applied this method to the correlation length results. In figure 6 we show $A_\xi(x_t)$ for the exponent $\nu = 0.671$ and various $L$-values. We note that already at $x_t \approx 4$ a plateau is reached and essentially no corrections to scaling are visible. The marginal spread of the data in the plateau region leads only to a small error for the amplitude $\xi^+$. Since the scaling variable $x_t$ changes with $\nu$ there is however a $\nu$-dependence, which can also be expressed as a dependence on $\alpha$, because of the hyperscaling relation $2 - \alpha = \mathrm{d}\nu$. In fact, after evaluating $A_\xi$ for several $\nu$-values, we find that $\xi^+$ is rather exactly a linear function of the $\alpha$ used:

$$\xi^+ = 0.4957(20) + 0.67(12)\alpha. \tag{44}$$

This can be seen in figure 7, where we compare the fit, equation (44), with some directly determined $\xi^+$-values.

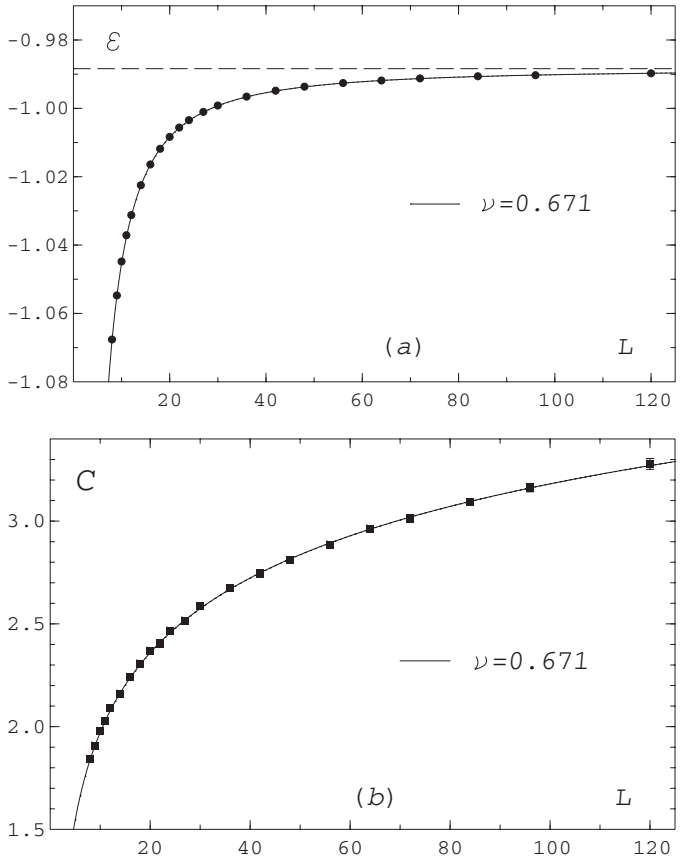


**Figure 8.** The energy density ($a$) and the specific heat ($b$) versus $L$ at the critical point. The dashed line shows $\epsilon_{ns}$ and the solid lines show fits to equations (45) and (46) for $\nu = 0.671$ and $\omega = 0.79$.

### *3.3. Specific heat and energy density at $T_c$*

As mentioned already in section 2, both the energy density and the specific heat contain additional non-singular terms. This fact complicates of course the determination of the critical amplitudes. We can however calculate the non-singular terms beforehand by a finite-size-scaling analysis directly at the critical point. For this purpose, we have made further Monte Carlo runs at $T_c$ on 23 lattices with $L = 8$ to $L = 160$. In these runs, we took between 500 000 and 200 000 measurements each for $L = 8$–64 and on the larger lattices between 120 000 and 50 000. The data for the energy density and the specific heat are shown in figure 8 as a function of $L$ up to $L = 120$. If one expands the scaling functions for $\epsilon$ and $C$ at $T_c$ in powers of $L^{-\omega}$, one obtains

$$\epsilon(L) = \epsilon_{ns} + q_{0\epsilon} L^{(\alpha-1)/\nu}(1 + q_{1\epsilon} L^{-\omega} + \cdots) \tag{45}$$

$$C(L) = C_{ns} + q_{0C} L^{\alpha/\nu}(1 + q_{1C} L^{-\omega} + \cdots). \tag{46}$$

We have fitted the first terms (up to $q_1$) of these expansions to the data. In the case of the energy density, we find no corrections to scaling, that is $q_{1\epsilon} \approx 0$ and only small corrections for the specific heat. Fits with different $\nu$-values cannot be distinguished in figure 8. When we

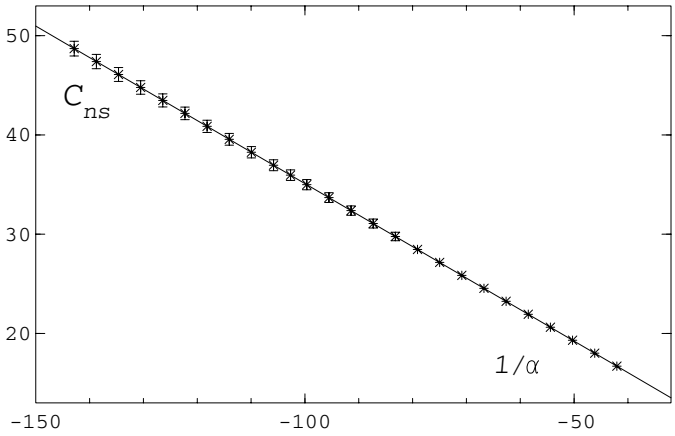


**Figure 9.** The non-singular part $C_{ns}$ of the specific heat versus $1/\alpha$ from fits to equation (46) (stars) with $\omega = 0.79$. The solid line is from equation (54).

treat $\nu$ as a free fit parameter we get $\nu = 0.671(2)$. The quantity $\epsilon_{ns}$ exhibits no noticeable dependence on $\nu$ or $\alpha$ and $\omega$. We find

$$\epsilon_{ns} = -0.988\,41(3). \tag{47}$$

The situation is quite different in the case of the specific heat. Its non-singular part varies from about 50 for $\nu = 0.669$ to 16 at $\nu = 0.675$. The reason for this strong variation is that the exponent $\alpha = 2 - 3\nu$ is close to zero, when $\nu$ approaches $2/3$. Then the background term $C_{ns}$ develops a pole ($\sim 1/\alpha$) which cancels a corresponding pole in the critical amplitude in such a way that the characteristic critical power behaviour ($\sim |t|^{-\alpha}$) turns over into a logarithmic behaviour ($\sim \ln |t|$).

This mechanism for the emergence of the logarithmic singularity as $\alpha \to 0$ is well known (see [15, 19, 20]). We demonstrate it by assuming that

$$C_{ns}(\alpha) = c_{ns}^0 + \frac{c_{ns}^p}{\alpha} \tag{48}$$

$$A^{\pm}(\alpha) = a_0^{\pm} + a_1^{\pm}\alpha + O(\alpha^2). \tag{49}$$

If we insert these equations into equation (22) and expand $|t|^{-\alpha}$ for small $\alpha$, we obtain

$$C = c_{ns}^0 + \frac{c_{ns}^p}{\alpha} + \left(\frac{a_0^{\pm}}{\alpha} + a_1^{\pm} + O(\alpha)\right)(1 - \alpha \ln |t| + \cdots) \tag{50}$$

$$= c_{ns}^0 + \frac{c_{ns}^p + a_0^{\pm}}{\alpha} + a_1^{\pm} - a_0^{\pm} \ln |t| + O(\alpha). \tag{51}$$

Evidently, the limit of $C$ for $\alpha \to 0$ exists and has a logarithmic $|t|$-dependence, if the pole term vanishes, which requires [19]

$$c_{ns}^p = -a_0^{\pm} \qquad \text{and} \qquad a_0^+ = a_0^-. \tag{52}$$

The ratio $A^+/A^-$ is therefore close to 1,

$$A^+/A^- = 1 + O(\alpha). \tag{53}$$

In figure 9 we show the non-singular part $C_{ns}$ of the specific heat resulting from fits to equation (46) with $\omega = 0.79$ and various values for $\alpha$ plotted versus $1/\alpha$. The $\chi^2$ per degree

of freedom in each fit is 0.83(1), preferring no particular $\alpha$-value. We see that indeed $C_{ns}$ is linearly dependent on $1/\alpha$. A fit to the ansatz, equation (48), gives

$$C_{ns} = 3.35(4) - \frac{0.3175(5)}{\alpha} \tag{54}$$

with an extremely small $\chi^2/N_f$ of the order of $10^{-4}$. We conclude from this fact, that the pole term behaviour of $C_{ns}$ is not a numerical accident, but underlines the previous considerations. In order to study the influence of the correction exponent $\omega$ we have repeated the whole analysis of $C(L)$ for the values $\omega = 0.77$ and $\omega = 0.81$, that is a standard deviation away from the central value 0.79. The $\chi^2/N_f$ for each single fit to equation (46) is again 0.83(1), the new values for $C_{ns}$ coincide within error bars with the values for $\omega = 0.79$, however the resultant linear fits in $1/\alpha$ to equation (48) at fixed $\omega$ lead to slight changes (again with a $\chi^2/N_f$ of the order of $10^{-4}$)

$$C_{ns} = \begin{cases} 3.37(4) - 0.3165(5)/\alpha & \text{for} \quad \omega = 0.77 \\ 3.33(4) - 0.3184(5)/\alpha & \text{for} \quad \omega = 0.81 \end{cases} \tag{55}$$

mainly for the pole term parameter $c_{ns}^p$.

In the following, we shall use the results for $C_{ns}$ to analyse as well the specific heat data for $T \neq T_c$. If not explicitly mentioned, the fit results have always been obtained for fixed $\omega = 0.79$. We have repeated the following analysis also for $\omega = 0.77$ and 0.81 and shall comment on any noticeable changes due to $\omega$.

### *3.4. The specific heat and $A^+/A^-$*

In figure 10 we have collected all of our specific heat data at zero magnetic field for the $L$-values of table 1. We observe with increasing $L$ a more and more pronounced peak close to $J_c$. As already discussed in the introduction, we nevertheless expect a finite peak height even in the thermodynamic limit, since the singular part of $C$ vanishes at the critical point for negative $\alpha$. The peak (and not dip) behaviour implies also that the amplitude $A^{\pm}/\alpha$ must be negative, or that $A^{\pm}$ is positive. The previous analysis of the non-singular contribution to $C$ confirms this consideration: because $c_{ns}^p$ is negative, we have a positive value $a_0^{\pm} = a_0$ for the leading part of $A^{\pm}$. We have interpolated the data points by reweighting, apart from the $L = 120$ results. The respective curves are plotted in figure 11 as a function of $t$. Compared to figure 10 we have therefore an exchange of the high- ($t > 0$, $J < 0$) and low-temperature ($t < 0$, $J > 0$) parts in the figures. In order to find the amplitudes $A^{\pm}$ we have made the following ansatz including correction-to-scaling terms,

$$C = C_{ns} + \frac{A^{\pm}}{\alpha}|t|^{-\alpha}\left(1 + c_1^{\pm}|t|^{\omega\nu} + c_2^{\pm}t\right). \tag{56}$$

For a fit to the form (56) the curves from the largest lattices were used in those $t$-ranges which appear hatched in figure 11, that is for $-0.0233 \leqslant t \leqslant -0.0045$ and $0.0048 \leqslant t \leqslant 0.0268$. The non-singular part from equation (54) was then taken as an input to the fit, whereas the $L = 120$ data points served only as a check of the fit result. As an example we show in figure 11 the fit for $\alpha = -0.013$. Fits with other small, negative $\alpha$-values work as well and have the same $\chi^2$ per degree of freedom, namely 1.03. In table 2 we present details of the fits for several $\alpha$-values. The two correction-to-scaling contributions are always opposite in sign and cancel therefore to some extent, especially in the high-temperature region. The amplitudes $A^{\pm}$ are still $\alpha$-dependent, though in our notation we have already taken the anticipated pole behaviour into account. We find that $A^+$ and $A^-$ are nearly linear functions of $\alpha$.

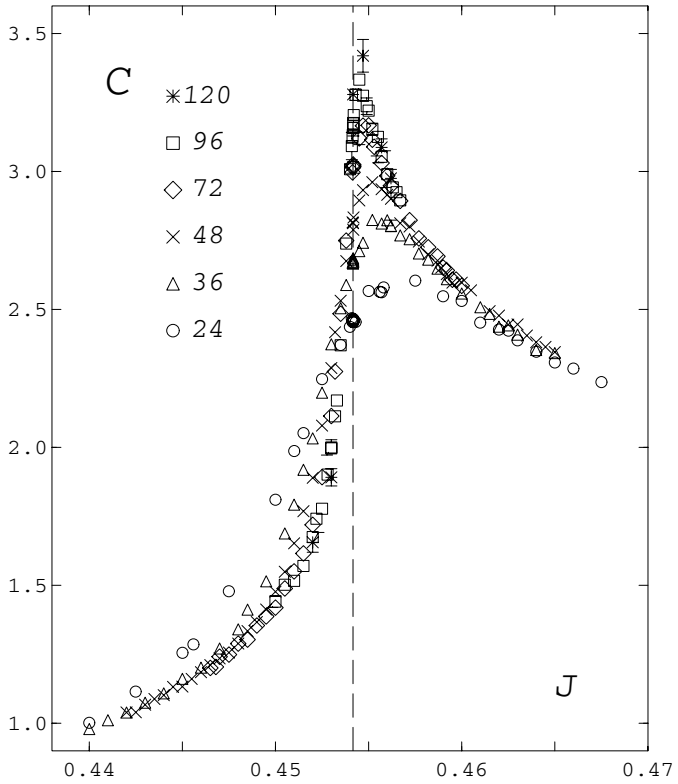


**Figure 10.** The specific heat data for different $L$ versus the coupling $J$. The dashed line indicates the position of the critical point.

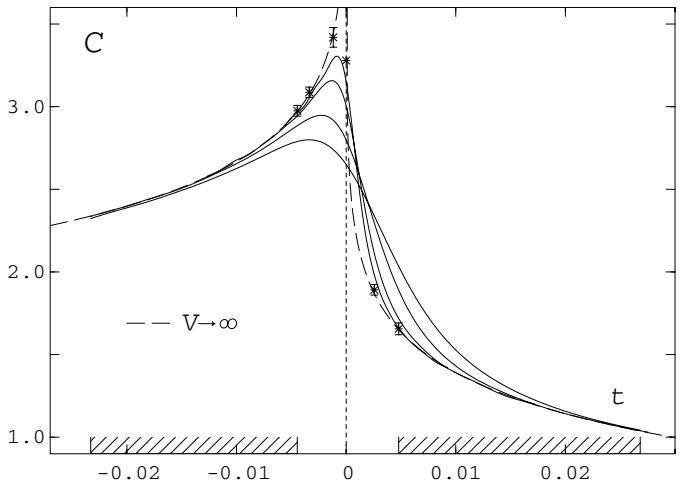


**Figure 11.** The specific heat versus the reduced temperature $t$ for $L = 36$, 48, 72, 96 and 120 (stars). The solid lines were calculated by reweighting the data; the peak height increases with $L$. The line with long dashes is the fit from the ansatz, equation (56), for $\alpha = -0.013$ and $\omega = 0.79$. The hatched areas show the fit regions.

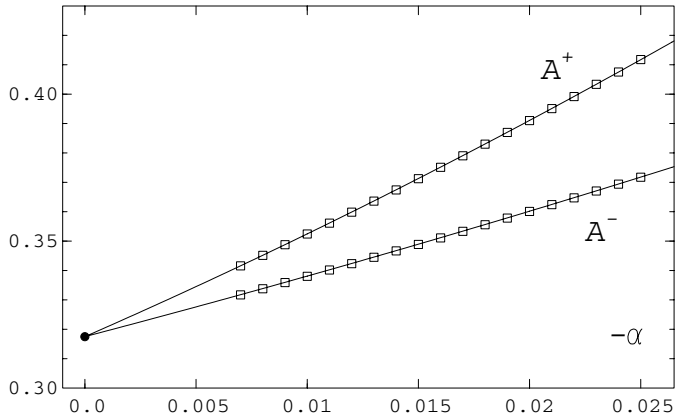


**Figure 12.** The amplitudes $A^+$ and $A^-$ versus $-\alpha$ (squares). The full circle is the value expected from $C_{ns}$; the lines are the parametrizations (58) and (59).

**Table 2.** The parameters of the fits to equation (56) for $\omega = 0.79$ and some selected $\alpha$-values. The errors were obtained by Monte Carlo variation of the parameters of $C_{ns}$ in equation (54).

| $\alpha$ | $A^+$ | $c_1^+$ | $c_2^+$ | $A^-$ | $c_1^-$ | $c_2^-$ |
|---|---|---|---|---|---|---|
| −0.007 | 0.3416(4) | 0.020(1) | −0.041(1) | 0.3317(4) | 0.048(1) | 0.086(1) |
| −0.013 | 0.3636(6) | 0.022(1) | −0.049(2) | 0.3445(6) | 0.085(1) | 0.161(2) |
| −0.017 | 0.3790(8) | 0.015(1) | −0.041(3) | 0.3533(8) | 0.109(2) | 0.211(4) |
| −0.019 | 0.3870(9) | 0.010(2) | −0.033(4) | 0.3578(9) | 0.120(2) | 0.237(5) |
| −0.025 | 0.4117(13) | −0.016(3) | 0.006(6) | 0.3718(13) | 0.151(4) | 0.312(9) |

The $\alpha$-dependence of the fit results for the amplitudes is shown in figure 12. A parametrization of the amplitudes as suggested by equations (49) and (52),

$$A^{\pm} = a_0 + a_1^{\pm}\alpha + a_2^{\pm}\alpha^2 \tag{57}$$

works extremely well, as can be seen in figure 12, and confirms explicitly the cancellation of the pole terms as predicted in equation (52). If $A^+$ and $A^-$ are independently fitted, that is with perhaps different $a_0$, we get $a_0^+ = 0.3176(12)$ and $a_0^- = 0.3175(12)$. The final result is found by using equation (57) with fixed $a_0 = 0.3175$ (the error in $a_0 = -c_{ns}^p$ is already included in the errors of the $A^{\pm}$-values, which are now parametrized). We obtain

$$A^+ = a_0 - 3.308(36)\alpha + 18.4(2.2)\alpha^2 \tag{58}$$

$$A^- = a_0 - 1.975(36)\alpha + 7.8(2.2)\alpha^2. \tag{59}$$

At this point it is appropriate to discuss the influence of an $\omega$-variation on $A^+$ and $A^-$. From equation (55) we know that a shift in $\omega$ of size $\Delta\omega = 0.02$ shifts the pole term parameter $c_{ns}^p$ by about 0.3% and therefore we expect a shift of $a_0$ by the same amount. In fact that is exactly what happens and it is the only effect, because the new parameters $a_1^{\pm}$ and $a_2^{\pm}$ coincide inside error bars with the values found for $\omega = 0.79$. All in all that results in a common shift of the $A^+$- and $A^-$-curves in figure 12 by again 0.3%. As a consequence, the universal amplitude ratio $A^+/A^-$ becomes essentially independent of $\omega$.

The universal ratio $A^+/A^-$ is sometimes given in terms of a function $\mathcal{P}(\alpha)$ [21],

$$A^+/A^- = 1 - \mathcal{P}\alpha. \tag{60}$$

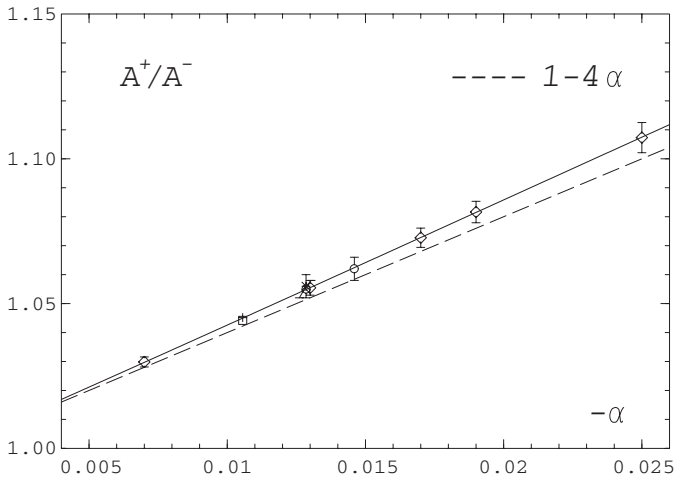


**Figure 13.** The universal ratio $A^+/A^-$ versus $-\alpha$. The solid line is obtained from equations (58) and (59), and the diamonds are by direct calculation from table 2. The other symbols denote results from the shuttle experiment (square) [7, 8], from Campostrini *et al* (circles) [10, 11], from Larin *et al* (star) [24] and Kleinert *et al* (plus) [25].

Expanding the ratio in powers of $\alpha$ we arrive at the following relation for $\mathcal{P}(\alpha)$:

$$\mathcal{P} = \frac{1}{\alpha}\left(1 - \frac{A^+}{A^-}\right) = \frac{a_1^- - a_1^+}{a_0} + \left[\frac{a_2^- - a_2^+}{a_0} - \frac{a_1^-}{a_0}\frac{a_1^- - a_1^+}{a_0}\right]\alpha + \cdots \tag{61}$$

that is $\mathcal{P}$ goes to a finite limit when $\alpha \to 0$ [21, 22]. In fact, there is a phenomenological relation [9, 23]

$$A^+/A^- = 1 - 4\alpha \tag{62}$$

predicting $\mathcal{P} = 4$. Evaluating equations (58) and (59) leads to

$$A^+/A^- = 1 - 4.20(5)\alpha + \cdots \tag{63}$$

rather close to relation (62). In figure 13 we show the ratio and compare it with former results from the shuttle experiment [7, 8] as well as some analytical determinations [10, 11, 24, 25]. We note that our ratio result is in complete accordance with all of the other ratio results. Obviously, they differ among each other simply and solely by assuming different $\alpha$-values. This conclusion was already reached by Campostrini *et al* [10]; we can however directly confirm it with equations (58) and (59).

## 4. $A^+/A^-$ from the equation of state

The magnetic equation of state describes the critical behaviour of the magnetization in the vicinity of $T_c$. As already noted by Widom [19] and Griffiths [22] long ago, the equation of state may be integrated to yield the scaling function for the free energy. From subsequent derivatives with respect to the temperature, one obtains then the specific heat and in particular an equation for the universal ratio $A^+/A^-$. Before we come to this relation, we must briefly discuss the equation of state. The Widom–Griffiths form of the equation of state is given by

$$y = f(x) \tag{64}$$

where

$$y \equiv h/M^\delta \qquad x \equiv \bar{t}/M^{1/\beta}. \tag{65}$$

The variables $\bar{t}$ and $h$ are the normalized reduced temperature and magnetic field,

$$\bar{t} = (T - T_c)/T_0 \qquad h = H/H_0 \tag{66}$$

associated with the usual normalization conditions

$$f(0) = 1 \qquad \text{and} \qquad f(-1) = 0. \tag{67}$$

The reduced temperature $\bar{t}$ differs from $t$ by a constant factor ($\bar{t} = [T_c/T_0]t$), because of the second condition in (67). The normalization constants can be expressed in terms of the critical amplitudes from equation (32),

$$T_0 = B^{-1/\beta} T_c = 1.18(2) \qquad H_0 = D_c = 1.11(1). \tag{68}$$

The numbers in the last equation have been obtained in [13] by assuming a special set [12] of critical exponents

$$\beta = 0.3490(6) \qquad \nu = 0.6723(11) \tag{69}$$

which implies $\alpha \approx -0.017$. The same is true for the equation of state, which was determined numerically in [13] from simulations with a non-zero magnetic field. Using this equation of state will therefore give $A^+/A^-$ for only that particular value of $\alpha$. Varying $\alpha$ in the range $[-0.0136, -0.0202]$, as suggested by the error of $\nu$, would result in a large variation of $A^+/A^-$ to begin with (see figure 13). Insofar, we consider the following calculation mainly as a test of the method.

The results for the equation of state were parametrized in [13] by a combination of a small-$x$ (low-temperature) and a large-$x$ (high-temperature) ansatz. The small-$x$ form $x_s(y)$ was inspired by perturbation theory [26] and incorporates the divergence of the susceptibility on the coexistence line ($x = -1$; $y = 0$) due to the massless Goldstone modes,

$$x_s(y) + 1 = (\widetilde{c}_1 + \widetilde{d}_3)y + \widetilde{c}_2 y^{1/2} + \widetilde{d}_2 y^{3/2}. \tag{70}$$

The large-$x$ form $x_l(y)$ was derived from Griffiths's analyticity condition [22]

$$x_l(y) = a y^{1/\gamma} + b y^{(1-2\beta)/\gamma}. \tag{71}$$

The parameter values are

$$\widetilde{c}_1 + \widetilde{d}_3 = 0.352(30) \qquad \widetilde{c}_2 = 0.592(10) \tag{72}$$

$$a = 1.2595(30) \qquad b = -1.163(20). \tag{73}$$

Because of the normalization $y(0) = 1$ we have $\widetilde{d}_2 = 1 - (\widetilde{c}_1 + \widetilde{d}_3 + \widetilde{c}_2)$. The complete equation of state is obtained by interpolation of the low- and high-temperature parts,

$$x(y) = x_s(y)\frac{y_0^p}{y_0^p + y^p} + x_l(y)\frac{y^p}{y_0^p + y^p} \tag{74}$$

with $p = 6$ and $y_0 = 3.5$.

For negative $\alpha$ the universal ratio $A^+/A^-$ can be calculated from $f(x)$ using the following formula [27]:

$$\frac{A^+}{A^-} = \frac{-\int_0^\infty \mathrm{d}x\, x^{\alpha-2}[f'(0) - f'(x) + f''(0)x]}{f'(0)/(1-\alpha) + f''(0)/\alpha + \int_{-1}^0 \mathrm{d}x(-x)^{\alpha-2}[f'(0) - f'(x) + f''(0)x]}. \tag{75}$$

The main contribution to both the nominator and the denominator is $f''(0)/\alpha$. A more appropriate representation of $A^+/A^-$ is therefore

$$\frac{A^+}{A^-} = \frac{1 + [\alpha/f''(0)]F_N}{1 + [\alpha/f''(0)]F_D} \tag{76}$$

where

$$F_N = -\frac{f'(0)}{1-\alpha} - \int_0^1 \mathrm{d}x\, x^{\alpha-2}[f'(0) - f'(x) + f''(0)x] + \int_1^\infty \mathrm{d}x\, x^{\alpha-2} f'(x) \tag{77}$$

$$F_D = \frac{f'(0)}{1-\alpha} + \int_{-1}^0 \mathrm{d}x(-x)^{\alpha-2}[f'(0) - f'(x) + f''(0)x]. \tag{78}$$

Let us denote the integrals in equation (77) by $I_1$ and $I_2$, and that in equation (78) by $I_3$. To a good approximation, we can calculate the integrals $I_1$ and $I_3$ as well as the derivatives from the low-temperature equation (70). In order to obtain $I_2$ we first rewrite the integral as

$$I_2 = -f(1) + (2-\alpha)\int_{f(1)}^\infty \mathrm{d}y\, y \frac{\mathrm{d}x}{\mathrm{d}y} x^{\alpha-3} \tag{79}$$

and evaluate the remaining integral from the interpolation formula (74), using for $f(1)$ the low-temperature value 2.4448. For the derivatives, we find

$$f'(0) = 2(3 - \widetilde{c}_1 - \widetilde{d}_3 - 2\widetilde{c}_2)^{-1} = 1.366 \pm 0.034 \tag{80}$$

$$f''(0) = [f'(0)]^3 \left(\tfrac{3}{4}(\widetilde{c}_1 + \widetilde{d}_3 - 1) + \widetilde{c}_2\right) = 0.270 \pm 0.064 \tag{81}$$

and for the integrals

$$I_1 = 0.203 \pm 0.02 \qquad I_2 = 1.749 \pm 0.03 \qquad I_3 = 0.512 \pm 0.02. \tag{82}$$

The errors in the integrals were obtained by Monte Carlo variation of the initial parameters in equations (72) and (73). When this procedure is also applied to the complete expression (76) one obtains

$$A^+/A^- = 1.12 \pm 0.05. \tag{83}$$

The first conclusion to be drawn from this result is that this method is not well suited for the calculation of the ratio, at least with the parametrization of the equation of state from [13]. Though the result (83) is compatible with our directly determined ratio $A^+/A^-\,(\alpha = -0.017) = 1.073(3)$, the error is rather large. The main source of the error is evidently the inaccurate value of $f''(0)$. That this quantity plays an important role is of course not unexpected, because $A^+$ and $A^-$ are the amplitudes of the specific heat, which is again the second derivative of the free energy density. Our parametrization was not devised for that purpose, but for a correct description of the Goldstone effect near $x = -1$ and the limiting behaviour for $x \to \infty$. That is why it led to a precise determination of $R_\chi$ and the constant $c_f$:

$$R_\chi = \lim_{x\to\infty} x^\gamma / f(x) = 1.356(4) \qquad c_f \equiv \lim_{x\to -1} (1+x)^{-2} f(x) = 2.85(7). \tag{84}$$

Campostrini *et al* have used a different representation of the equation of state [28, 11], based on Josephson's parametrization [29] of $M$, $\bar{t}$ and $H$ in terms of the variables $R$ and $\theta$ and parametric functions. In order to fix these functions approximately, the authors utilized the results of an analysis of the high-temperature expansion of an improved lattice Hamiltonian. The values obtained for $A^+/A^-$ compare well with our direct determination and have already been shown in figure 13. The corresponding equation of state differs, however, somewhat in the low- and medium-temperature regions from the data points in our non-zero field simulations [13]. The question arises then whether the same data may be described as well in the schemes introduced by Campostrini *et al*. Such alternative fits of the data have been carried out by two of us [30]. The $\chi^2$ per degree of freedom of these fits is generally high, in particular for scheme $A$ of [28]. The fits according to scheme $B$ are considerably better and lead to a ratio

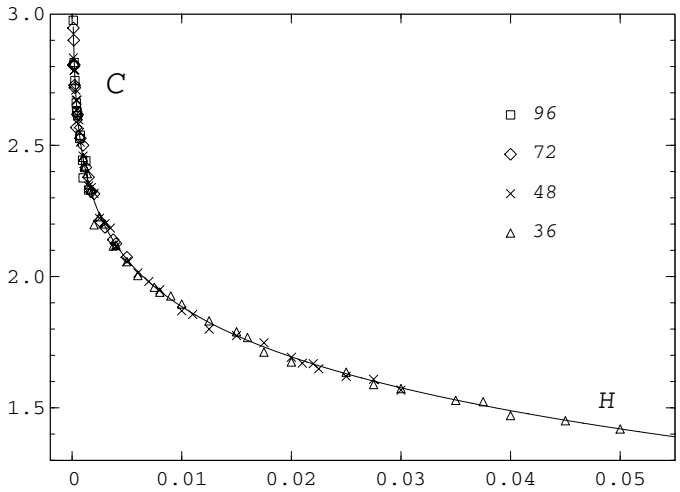


**Figure 14.** The specific heat at $T_c$ for $L = 36, 48, 72$ and 96 as a function of $H$. The line is the fit (85) for $\alpha_c = -0.0078$ ($\nu = 0.671$) and $\omega = 0.79$.

**Table 3.** Survey of the new Monte Carlo simulations at $T_c$ on different lattices. $N_{\mathrm{cu}}$ is the number of cluster updates between the measurements, $N_{\mathrm{meas}}$ the number of measurements per $H$-value in units of 1000 and $N_H$ the number of $H$-values at which new runs were performed. $N_{\mathrm{tot}}$ is the total number of $H$-values where we have data.

| $L$ | $H$-range | $N_{\mathrm{cu}}$ | $N_{\mathrm{meas}}(1000)$ | $N_H$ | $N_{\mathrm{tot}}$ |
|---|---|---|---|---|---|
| 36 | 0.0007–0.05 | 50–100 | 30–40 | 25 | 36 |
| 48 | 0.0001–0.03 | 50–100 | 30–40 | 30 | 39 |
| 72 | 0.0001–0.005 | 60–300 | 20 | 15 | 23 |
| 96 | 0.0001–0.0015 | 60–80 | 12–20 | 8 | 16 |

$A^+/A^- = 1.070(13)$, again compatible with our direct determination. The simultaneously calculated ratio $R_C$ is however much larger (0.165–0.185) than expected from analytical calculations (0.123–0.130) [31, 25]. We therefore do not pursue this method of calculation here in more detail.

## 5. Simulations with $H > 0$

We have performed additional simulations with a positive magnetic field $H$ on the critical line to find the remaining critical amplitudes for the specific heat and the longitudinal and transverse correlation lengths. The linear extensions of the lattices we used were $L = 36, 48, 72$ and 96. These measurements were combined with those from [13] to cover the $H$-range appropriately. Some of the new data have already been used in [32]. In table 3 we give more details of these simulations.

### *5.1. The specific heat on the critical line*

In figure 14 we show our specific heat data as a function of the magnetic field $H$. Since there are no noticeable systematic finite-size effects, we can use these data to fit them to the ansatz

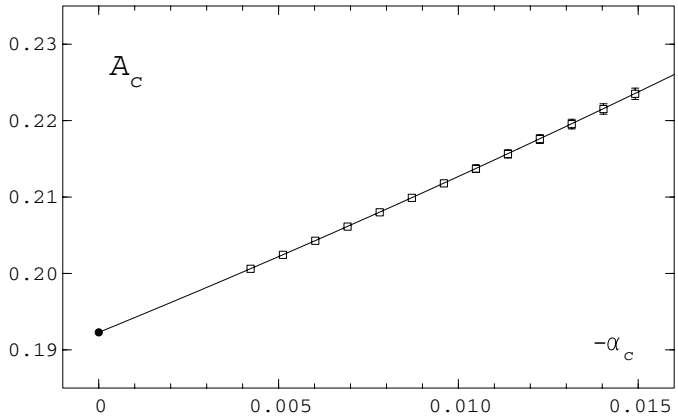


**Figure 15.** The amplitude $A_c$ versus $-\alpha_c$ (squares) for $\omega = 0.79$. The full circle shows the value expected from $C_{ns}$; the line is the parametrization (89).

**Table 4.** The parameters of the fits to equation (85) for some selected $\alpha_c$-values at fixed $\beta = 0.349$ and $\omega = 0.79$. The errors were obtained by Monte Carlo variation of the parameters of $C_{ns}$ in equation (88).

| $\alpha_c$ | $\alpha$ | $A_c$ | $c_h$ | $\chi^2/N_f$ |
|---|---|---|---|---|
| −0.004 22 | −0.007 | 0.2006(2) | 0.0203(1) | 1.09 |
| −0.007 81 | −0.013 | 0.2080(3) | 0.0344(2) | 1.09 |
| −0.010 19 | −0.017 | 0.2131(5) | 0.0423(4) | 1.10 |
| −0.011 38 | −0.019 | 0.2156(5) | 0.0458(4) | 1.10 |
| −0.014 92 | −0.025 | 0.2235(7) | 0.0546(8) | 1.11 |

$$C = C_{ns} + \frac{A_c}{\alpha_c} H^{-\alpha_c}(1 + c_h H^{\omega\nu_c}). \tag{85}$$

Here, $C_{ns}$ is the same non-singular term, which we have already determined in section 3.3 as a function of $\alpha$ (or $\nu$) with the result (54). Because of the dependence of $C$ on $\alpha_c$ and $\nu_c$ the amplitudes $A_c$ and $c_h$ depend on two critical exponents. The second exponent will not however introduce a sizeable variation in the amplitudes. We therefore treat the exponent $\beta$ as fixed at the value $\beta = 0.349$, in accord with our previous calculations. With the relations

$$\beta\delta = 2 - \beta - \alpha \qquad \alpha_c = \frac{\alpha}{2 - \beta - \alpha} \qquad \alpha = \frac{\alpha_c(2 - \beta)}{1 + \alpha_c} \tag{86}$$

the linear dependence of $C_{ns}$ on $1/\alpha$ can be rewritten as one on $1/\alpha_c$:

$$C_{ns} = c_{ns}^0 + \frac{c_{ns}^p}{2 - \beta}\left(1 + \frac{1}{\alpha_c}\right) \tag{87}$$

$$= 3.16(4) - \frac{0.1923(3)}{\alpha_c}. \tag{88}$$

We took this form of $C_{ns}$ as an input to the fits of $C$ with equation (85). The $H$-range for the fits was $0.0001 \leqslant H \leqslant 0.05$. We have convinced ourselves that smaller $H$-ranges (up to 0.02 or 0.03) lead inside the error bars to the same results for the amplitudes. In table 4 we present details of the fits for several $\alpha_c$-values, and in figure 15 we show the amplitude $A_c$ as a function of $\alpha_c$. As in the case of the amplitudes $A^{\pm}$ the pole of $C_{ns}$ in equation (88) is

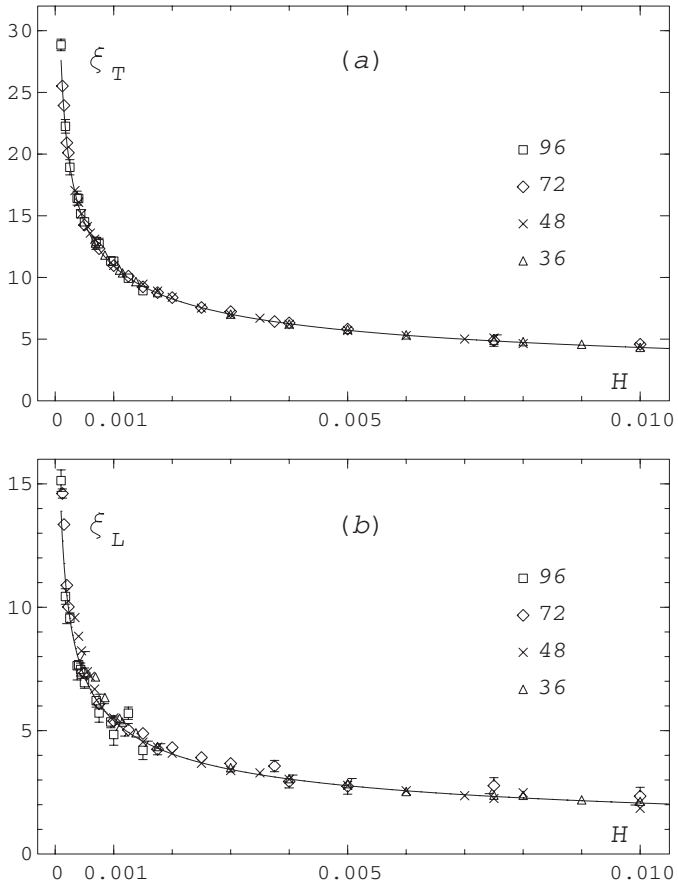


**Figure 16.** The correlation lengths $\xi_T$ ($a$) and $\xi_L$ ($b$) at $T_c$ for $L = 36, 48, 72$ and 96 as a function of $H$. The lines are the fits (90) for $\nu_c = 0.403\,25$ and $\omega = 0.79$.

compensated by the corresponding pole term in $A_c/\alpha_c$. We have therefore parametrized the $\alpha_c$-dependence of $A_c$ in analogy to equation (57) with the fixed value $A_c\,(\alpha_c = 0) = 0.1923$ and find

$$A_c = 0.1923 - 1.919(42)\alpha_c + 11.6(4.1)\alpha_c^2. \tag{89}$$

From figure 15 we see that this parametrization describes the data very well. As in the study of the $\omega$-dependence of $A^{\pm}$ in section 3.4 we found changes of similar size for the amplitude $A_c$ due to a variation of $\omega$. They lead to an additional error of $A_c$ of size 0.0006 at $\alpha_c = -0.004\,22$, which decreases to 0.0004 at $\alpha_c = -0.014\,92$.

### *5.2. The correlation lengths on the critical line*

The simulation results for the transverse and longitudinal correlation lengths are shown in figures 16($a$) and ($b$). For the transverse correlation length $\xi_T$ one can hardly detect finite-size effects, whereas the longitudinal correlation length $\xi_L$ shows more fluctuations and a systematic deviation to higher $\xi_L$-values, when one decreases the magnetic field $H$. The smaller the lattice,

**Table 5.** The parameters of the fits to equation (90) for some selected $\nu_c$-values and $\omega = 0.79$. The $\chi^2/N_f$-values varied for $\xi_T$ between 0.89 and 0.86; for $\xi_L$ it was 0.67.

| $\nu_c$ | $\alpha$ | $\xi_T^c$ | $c_T$ | $\xi_L^c$ | $c_L$ |
|---|---|---|---|---|---|
| 0.403 50 | −0.007 | 0.6709(14) | 0.024(13) | 0.3427(15) | −0.258(33) |
| 0.403 25 | −0.013 | 0.6724(14) | 0.019(14) | 0.3435(15) | −0.263(33) |
| 0.403 07 | −0.017 | 0.6735(14) | 0.015(14) | 0.3441(15) | −0.266(33) |
| 0.402 99 | −0.019 | 0.6740(14) | 0.013(14) | 0.3443(15) | −0.268(32) |
| 0.402 74 | −0.025 | 0.6755(14) | 0.008(14) | 0.3451(15) | −0.273(32) |

the earlier this behaviour sets in. In order to determine the amplitudes, we have fitted our results to the following form:

$$\xi_{T,L} = \xi_{T,L}^c H^{-\nu_c}(1 + c_{T,L} H^{\omega\nu_c}). \tag{90}$$

In the transverse case, we used the reweighted data for $L = 72$ in the $H$-interval [0.0005, 0.0025], for $L = 48$ in [0.002, 0.02] and for $L = 36$ in [0.015, 0.03]. From table 5 we see that the correction term is essentially zero. Correspondingly, there is no $\omega$-dependence and a fit with $c_T \equiv 0$ works just as well (even with the same $\chi^2/N_f$), and leads to a slight increase in the amplitude value, which is of the order of the error given in table 5. The dependence of the amplitude $\xi_T^c$ on $\nu_c$ or $\alpha$ is linear but the slope is very small. In order to determine the longitudinal amplitude $\xi_L^c$ we have fitted the reweighted data for $L = 72$ in the $H$-interval [0.0005, 0.001 75] together with those for $L = 48$ in [0.001 75, 0.01]. Here, the correction term is not zero, but the variation due to $\omega$ is still negligible. The $\nu_c$- or $\alpha$-dependence is the same as for $\xi_T^c$, and the ratio of the two correlation lengths is a fixed number

$$\xi_T^c/\xi_L^c = 1.957(10) \tag{91}$$

independent of the critical exponents. It is well known (see [15, 33, 34]) that at zero field on the coexistence line $t < 0$ the longitudinal correlation function $G_L$ is for large distances $|\vec{r}|$ connected to the transverse one by

$$G_L(\vec{r}, t) \approx \tfrac{1}{2}(N-1)[G_T(\vec{r}, t)/M]^2 \tag{92}$$

where in our case $N = 2$. The relation is expected to hold also for small non-zero fields $H$ near the phase boundary in the regime of exponential decay implying a factor 2 between the correlation lengths. It is remarkable that we find approximately such a value for the ratio at $t = 0$. A similar observation has been made for the 3D $O(4)$ model [35].

### *5.3. The stiffness constant on the coexistence line*

The stiffness constant $\rho_s(T)$ is related to the helicity modulus $\Upsilon$ [36] by

$$\rho_s = \Upsilon/T \tag{93}$$

which can be measured in Monte Carlo simulations. This was done, for example, in [37, 38]. Here we follow a different strategy, which we have already applied in [13] to find the magnetization on the coexistence line. The $L$ or volume dependence of $M$ at fixed $J$ and fixed small $H$ is described by the $\epsilon$-expansion of chiral perturbation theory (CPT) in terms of two low-energy constants. One is the Goldstone-boson-decay constant $F$, and the other is the magnetization $\Sigma$ of the continuum theory for $H = 0$ and $V \to \infty$. The square of the constant $F$ is proportional to the helicity modulus. In our notation, which is different from that in CPT (see the remark in the last paragraph of [39]) we have

$$\Upsilon = F^2/J \qquad \text{implying} \quad \rho_s = F^2. \tag{94}$$

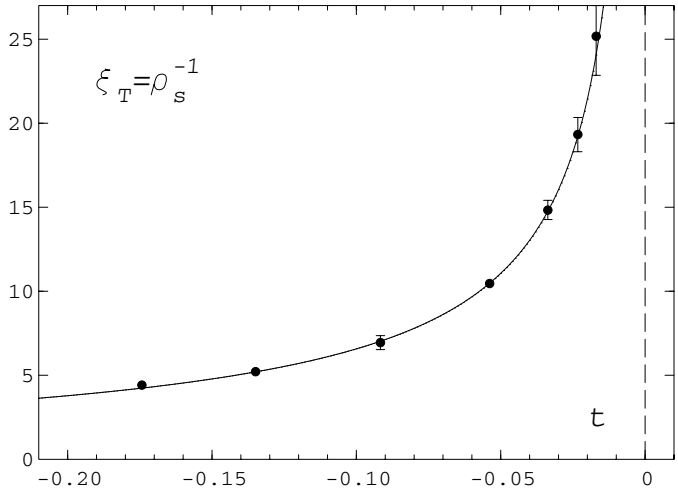


**Figure 17.** The inverse of the stiffness constant $\rho_s^{-1} = \xi_T$ on the coexistence line from chiral perturbation theory. The solid line is the fit (96) with $\nu = 0.671$ and $\omega = 0.79$.

**Table 6.** The Goldstone-boson-decay constant $F$ at various $J$-values from fits on data from lattices with $L$ in the range $[L_{\min}, L_{\max}]$.

| $J = 1/T$ | $F$ | $\Delta F$ | $L_{\min}$ | $L_{\max}$ |
|---|---|---|---|---|
| 0.462 | 0.1993 | 0.0096 | 8,10,12 | 36,40 |
| 0.465 | 0.2275 | 0.0060 | 8,10,12 | 40,48 |
| 0.470 | 0.2596 | 0.0050 | 8,10,12 | 40,48 |
| 0.480 | 0.3091 | 0.0018 | 8,10,12 | 48 |
| 0.500 | 0.3795 | 0.0114 | 8,10,12 | 48,56 |
| 0.525 | 0.4379 | 0.0040 | 8,10,12 | 48,56 |
| 0.550 | 0.4755 | 0.0028 | 8,10,12 | 56 |

The formulae, which are needed for the fits to determine the constants, are summarized in [13] and were taken from [39]. In table 6 we list the results for the Goldstone-boson-decay constant $F$ at various $J$-values. We performed simulations at $H = 0.0001$ on lattices with linear extensions $L = 8, 10, 12, 16, 20, 24, 30, 36, 40, 48$ and 56. By construction, the $\epsilon$-expansion is only applicable in a range where $m_\pi L \lesssim 1$. This condition translates into the equation

$$H \frac{\Sigma}{\sqrt{J}} \lesssim \left(\frac{F}{L}\right)^2 \tag{95}$$

and excludes the use of too large $L$-values. For each $J$ we fitted different sets of data from lattices between $[L_{\min}, L_{\max}]$ and averaged the obtained $F$-values. The errors on $F$ include the variations of these results. If we compare our $F$-values with the corresponding values from [39] we find generally somewhat lower numbers. This may be due to the fact that the fits of [39] were performed for fixed-$L$ values only. The transverse correlation length $\xi_T$ on the coexistence line is now derived from the inverse of the stiffness constant or $F^{-2}$. It is plotted in figure 17. Here, we do not have as many and as accurate data as in figure 16($a$). In order to determine the amplitude $\xi_T^-$ we fit our data points up to $J = 0.525$ to the ansatz

$$\xi_T = \xi_T^-(-t)^{-\nu}(1 + c_T^-(-t)^{\omega\nu}). \tag{96}$$

**Table 7.** The parameters of the fits to equation (96) for several $\nu$-values and $\omega = 0.79$.

| $\nu$ | $\alpha$ | $\xi_T^-$ | $c_T^-$ | $\chi^2/N_f$ |
|---|---|---|---|---|
| 0.6690 | −0.007 | 1.680(52) | −0.55(10) | 0.08 |
| 0.6710 | −0.013 | 1.665(52) | −0.54(11) | 0.08 |
| 0.6723 | −0.017 | 1.655(51) | −0.53(11) | 0.08 |
| 0.6730 | −0.019 | 1.650(51) | −0.53(11) | 0.08 |
| 0.6750 | −0.025 | 1.636(51) | −0.52(11) | 0.07 |

**Table 8.** The universal ratios from equations (28), (29) and (30) as a function of the used exponents $\nu$ and $\alpha$.

| $\nu$ | $\alpha$ | $R_\xi^+$ | $R_\xi^T$ | $R_C$ | $R_A$ | $Q_2^T$ |
|---|---|---|---|---|---|---|
| 0.6690 | −0.007 | 0.3432(15) | 1.163(36) | 0.118(4) | 0.0515(17) | 0.834(21) |
| 0.6710 | −0.013 | 0.3476(18) | 1.167(36) | 0.125(4) | 0.0534(18) | 0.849(21) |
| 0.6723 | −0.017 | 0.3505(21) | 1.170(36) | 0.130(4) | 0.0547(18) | 0.860(21) |
| 0.6730 | −0.019 | 0.3520(22) | 1.171(36) | 0.133(5) | 0.0554(19) | 0.865(21) |
| 0.6750 | −0.025 | 0.3563(27) | 1.176(36) | 0.142(5) | 0.0574(19) | 0.881(22) |

Table 7 contains the fit parameters for different $\nu$ or $\alpha$-values. We observe, as for $\xi_T^c$, a linear dependence of the amplitude $\xi_T^-$ on $\alpha$ with a very small slope. A change in $\omega$ by 0.02 leads only to a shift in $\xi_T^-$ of a tenth of the error in table 7.

## 6. The universal amplitude ratios

After having determined all the amplitudes which appear in equations (27) to (30) we can calculate the corresponding universal ratios. Since the ratio $U_0 = A^+/A^-$ has already been discussed in great detail, we start with the ratio $U_\xi$ of the correlation lengths for $H = 0$. From equation (44) and table 7 we find

$$U_\xi = \xi^+/\xi_T^- = 0.293(9) \tag{97}$$

independent of the $\alpha$-value used. The $\epsilon$-expansion of this ratio was derived by Hohenberg *et al* [23] to $O(\epsilon)$ and extended by Bervillier [40] to $O(\epsilon^2)$ resulting in $U_\xi = 0.27$ and 0.33, respectively. Okabe and Ideura [41] corrected the expansion of Bervillier (not the numerical value) and computed the ratio in $1/N$-expansion to $U_\xi = 0.140$. The $\epsilon$-expansion results are comparable in size to our value in (97); the $1/N$-expansion result, however, seems to be too small.

The ratios connecting the specific heat and correlation length amplitudes are related by

$$R_\xi^+ = R_\xi^T {U_0}^{1/d} U_\xi \tag{98}$$

and they depend on the $\alpha$ used, mainly because of the specific heat amplitudes. In table 8 we have listed the ratios $R_\xi^+$ and $R_\xi^T$. From the $\alpha$-expansions (44) and (58) we find

$$R_\xi^+ = 0.3382(14) - 0.717(96)\alpha + 0.87(1.13)\alpha^2. \tag{99}$$

For $R_\xi^T$ one can derive a similar formula representing the values of table 8,

$$R_\xi^T = 1.1580 - 0.696\alpha + 0.97\alpha^2 \pm 0.036. \tag{100}$$

There exist several theoretical estimates of $R_\xi^+$ which compare well with our result: 0.355(3) ($\alpha = -0.0146$) [11] and 0.361(4) [42], both from high-temperature expansions; 0.36 [40]

from the $\epsilon$-expansion, and 0.3597(10) [43] and 0.3606(20) [44] from 3D field theory. Apart from the first result, we could not relate a definite $\alpha$-value to the respective estimate. The ratio $R_\xi^T$ was calculated from the $\epsilon$-expansion [23, 40] with the result 1.0(2) [15], well in accord with our value.

The remaining universal ratios $R_\chi$, $R_C$, $R_A$ and $Q_2^T$ are all dependent on the amplitude $C^+$ of the susceptibility and/or the amplitudes $B$ and $d_c(D_c)$ of the magnetization. We have already mentioned that we determined $R_\chi$, $B$ and $d_c$ in [13], although for fixed $\nu = 0.6723$. In the following we proceed as in section 5.1, that is we keep $\beta$ fixed at 0.349 and assume in addition that the $\nu$-dependences of $R_\chi$, $B$ and $d_c$ are negligible. In table 8 we present the ratios $R_C$ and $Q_2^T$ as calculated from

$$R_C = A^+ R_\chi D_c^{-1} B^{-1-\delta} \qquad Q_2^T = \left(\xi_T^c / \xi^+\right)^{\gamma/\nu} R_\chi (d_c/B)^{\delta-1}/(1+1/\delta) \tag{101}$$

and $R_A$ directly from the definition in equation (30), using our newly determined amplitudes $A^+$, $A_c$, $\xi_T^c$ and $\xi^+$. We could not find any previous results for $R_A$ and $Q_2^T$ in the literature; however, the ratio $R_C$ has been calculated theoretically in several ways. From table 8 we see that $R_C$ is increasing with decreasing $\alpha$, which is due to the factor $A^+$. In comparing our values to the analytical results, we quote therefore the $\alpha$-values used. The ratio $R_C$ calculated from 3D field theory in [31] is 0.123(3) ($\alpha = -0.012\,85$), in [25] 0.124 28 ($\alpha = -0.010\,56$); from the high-temperature expansion in [11] one finds 0.127(6) ($\alpha = -0.0146$). The results are in full agreement with our calculation, though the result of [25] is somewhat higher than the others. The old $\epsilon$-expansion result 0.103 of Aharony and Hohenberg [45] seems to be too small.

## 7. Conclusions

We have calculated the major universal amplitude ratios of the three-dimensional $O(2)$ model from Monte Carlo simulations. To reach this goal, a large amount of computer time had to be spent on the cluster of alpha-workstations of the department of physics at the University of Bielefeld. Most of the computer time went into the production of reliable specific heat data for the direct determination of $A^+/A^-$. Initially, we hoped to improve the accuracy of the exponent $\alpha$ (or $\nu$) from these data. As it turned out, however, the specific heat data could be fitted to a whole range of $\alpha$-values with the same $\chi^2/N_f$, extending even to $\alpha = 0$. This raises the question whether the experimental shuttle data are really fixing the $\alpha$-value to exactly $-0.010\,56$, the same value as in 3D field theory expansions [1]. The positive aspect of the indifference of the fits to the specific heat data to $\alpha$-variations was that we could study the numerical changes induced by these variations in the universal ratio $A^+/A^-$ and the background term $C_{ns}$. As a result, we were able to confirm the conjectured pole $(1/\alpha)$ behaviour of the amplitudes and the background term and the mutual cancellation of the pole contributions. The same pole behaviour was observed for the specific heat amplitude on the critical line. The functional dependence of $A^+/A^-$ on the $\alpha$-value used is in complete accordance with all other ratio results and not far from the phenomenological relation $A^+/A^- = 1 - 4\alpha$. We have also determined $A^+/A^-$ from the numerical equation of state, but we think that the method relies too much on the chosen parametrization.

In order to find the amplitude of the transverse correlation length on the coexistence line, we used chiral perturbation theory. This enabled us to calculate the less known ratios $R_\xi^T$ and $U_\xi$. The latter is independent of the $\alpha$ used, such as the ratio $\xi_T^c/\xi_L^c$ on the critical line, which is remarkably close to 2—a prediction expected for $T < T_c$ from the correlation functions close to the phase boundary. Our results for $R_\xi^+$ and $R_C$ are in full agreement with the best theoretical estimates; $R_A$ and $Q_2^T$ are new and remain untested for the moment.

## Acknowledgments

We are grateful to Jean Zinn-Justin, Michele Caselle, Martin Hasenbusch and Andrea Pelissetto for discussions and to Ettore Vicari for his comments on the calculation of $A^+/A^-$ from the equation of state. Our work was supported by the Deutsche Forschungsgemeinschaft under grant no FOR 339/1-2. In addition, the work of AC and TM was supported by FAPESP, Brazil (project no 00/05047-5).

## References

[1] Zinn-Justin J 2001 *Phys. Rep.* **344** 159 (*Preprint* hep-th/0002136)
[2] Le Guillou J C and Zinn-Justin J 1977 *Phys. Rev. Lett.* **39** 95
[3] Le Guillou J C and Zinn-Justin J 1980 *Phys. Rev.* B **21** 3976
[4] Guida R and Zinn-Justin J 1998 *J. Phys. A: Math. Gen.* **31** 8103 (*Preprint* cond-mat/9803240)
[5] Fairbank W M, Buckingham M J and Kellers C F 1957 *Proc. 5th Int. Conf. on Low Temp. Phys. (Madison, WI)* p 50
[6] Bagatskii M I, Voronel' A V and Gusak V G 1963 *Sov. Phys.–JETP* **16** 517
[7] Lipa J A, Swanson D R, Nissen J A, Chui T C P and Israelsson U E 1996 *Phys. Rev. Lett.* **76** 944
[8] Lipa J A, Swanson D R, Nissen J A, Geng Z K, Williamson P R, Stricker D A, Chui T C P, Israelsson U E and Larson M 2000 *Phys. Rev. Lett.* **84** 4894
[9] Pelissetto A and Vicari E 2000 *Preprint* cond-mat/0012164 (*Phys. Rep.* to be published)
[10] Campostrini M, Hasenbusch M, Pelissetto A, Rossi P and Vicari E 2001 *Nucl. Phys. Proc. Suppl.* **94** 857 (*Preprint* hep-lat/0010041)
[11] Campostrini M, Hasenbusch M, Pelissetto A, Rossi P and Vicari E 2001 *Phys. Rev.* B **63** 214503 (*Preprint* cond-mat/0010360)
[12] Hasenbusch M and Török T 1999 *J. Phys. A: Math. Gen.* **32** 6361 (*Preprint* cond-mat/9904408)
[13] Engels J, Holtmann S, Mendes T and Schulze T 2000 *Phys. Lett.* B **492** 219 (*Preprint* hep-lat/0006023)
[14] Talapov A L and Blöte H W 1996 *J. Phys. A: Math. Gen.* **29** 5727 (*Preprint* cond-mat/9603013)
[15] Privman V, Hohenberg P C and Aharony A 1991 *Phase Transitions and Critical Phenomena* vol 14 ed C Domb and J L Lebowitz (New York: Academic)
[16] Ballesteros H G, Fernández L A, Martín-Mayor V and Muñoz Sudupe A 1996 *Phys. Lett.* B **387** 125 (*Preprint* cond-mat/9606203)
[17] Arnold P and Moore G D 2001 *Phys. Rev.* E **64** 066113 (*Preprint* cond-mat/0103227)
[18] Engels J and Scheideler T 1999 *Nucl. Phys.* B **539** 557 (*Preprint* hep-lat/9808057)
[19] Widom B 1965 *J. Chem. Phys.* **43** 3898
[20] Wegner F J 1972 *Phys. Rev.* B **5** 4529
[21] Barmatz M, Hohenberg P C and Kornblit A 1975 *Phys. Rev.* B **12** 1947
[22] Griffiths R B 1967 *Phys. Rev.* **158** 176
[23] Hohenberg P C, Aharony A, Halperin B I and Siggia E D 1976 *Phys. Rev.* B **13** 2986
[24] Larin S A, Mönnigmann M, Strösser M and Dohm V 1998 *Phys. Rev.* B **58** 3394 (*Preprint* cond-mat/9711069)
[25] Kleinert H and Van den Bossche B 2001 *Phys. Rev.* E **63** 056113 (*Preprint* cond-mat/0011329)
[26] Wallace D J and Zia R K P 1975 *Phys. Rev.* B **12** 5340
[27] Aharony A and Bruce A D 1974 *Phys. Rev.* B **10** 2973
[28] Campostrini M, Pelissetto A, Rossi P and Vicari E 2000 *Phys. Rev.* B **62** 5843 (*Preprint* cond-mat/0001440)
[29] Josephson B D 1969 *J. Phys. C: Solid State Phys.* **2** 1113
[30] Cucchieri A and Mendes T to be published
[31] Strösser M, Larin S A and Dohm V 1999 *Nucl. Phys.* B **540** 654 (*Preprint* cond-mat/9806103)
[32] Engels J, Holtmann S, Mendes T and Schulze T 2001 *Phys. Lett.* B **514** 299 (*Preprint* hep-lat/0105028)
[33] Patashinskii A L and Pokrovskii V L 1973 *Zh. Eksp. Teor. Fiz.* **64** 1445 (Engl. Transl. Patashinskii A L and Pokrovskii V L 1974 *Sov. Phys.–JETP* **37** 733)
[34] Fisher M E and Privman V 1985 *Phys. Rev.* B **32** 447
[35] Fromme L 2002 Goldstone-Effekte und Korrelationslängen des dreidimensionalen O(4)-Spinmodells *Diploma thesis* Bielefeld University
[36] Fisher M E, Barber M N and Jasnow D 1973 *Phys. Rev.* A **8** 1111
[37] Li Y-H and Teitel S 1989 *Phys. Rev.* B **40** 9122
[38] Janke W 1990 *Phys. Lett.* A **148** 306

[39] Tominaga S and Yoneyama H 1995 *Phys. Rev.* B **51** 8243 (*Preprint* hep-lat/9408001)
[40] Bervillier C 1976 *Phys. Rev.* B **14** 4964
[41] Okabe Y and Ideura K 1981 *Prog. Theor. Phys.* **66** 1959
[42] Butera P and Comi M 1999 *Phys. Rev.* B **60** 6749 (*Preprint* hep-lat/9903010)
[43] Bervillier C and Godrèche C 1980 *Phys. Rev.* B **21** 5427
[44] Bagnuls C and Bervillier C 1985 *Phys. Rev.* B **32** 7209
[45] Aharony A and Hohenberg P C 1976 *Phys. Rev.* B **13** 3081